

UWB-Based Tracking of Autonomous Vehicles with Multiple Receivers

Stefano Busanelli and Gianluigi Ferrari

Wireless Ad-hoc and Sensor Networks (WASN) Lab,
Department of Information Engineering, University of Parma, Italy
busanelli@tlc.unipr.it, gianluigi.ferrari@unipr.it

Abstract. In this paper, we consider real-time tracking of an Autonomous Guided Vehicle (AGV) in an indoor industrial scenario. An on-board odometer provides information about the dynamic state of the AGV, allowing to predict its pose (position and orientation). At the same time, an external Ultra Wide Band (UWB) wireless network provides the information necessary to compensate the error drift accumulated by the odometer. Two novel alternative solutions for real-time tracking are proposed: (i) a classical Time Differences of Arrivals (TDOA) approach with a single receiver; (ii) a “Twin-receiver” TDOA (TTDOA) approach, that requires the presence of two independent receivers on the AGV. The performance of the two proposed algorithms is evaluated in realistic conditions. The obtained results clearly show the tradeoff existing between the frequency of UWB measurements and their quality.

1 Introduction

Following the pioneering work of Win and Scholtz [15], in the last years Ultra-Wide Band (UWB) impulse radio technology has appeared as a technology able to offer a high level of precision with limited costs, having the potential to implement GPS-like indoor positioning systems [6]. Because of the ability of UWB receivers to precisely measure the Time-Of-Arrival (TOA) or the Angle of Arrival (AOA) of UWB signals, this technology can guarantee a centimeter-grade (or even lower) precision [5]. The systems commercially available today are not far from these limits, since they claim a precision on the order to 10÷15 cm, despite the challenging indoor multi-path channel that characterizes most industrial buildings [14]. In the next future, thanks to the continuous improvements of electronics and upon the introduction of the IEEE 802.15.4a standard [1], there is hope that this technology will become more accurate, yet less expensive.

For Autonomous Guided Vehicle (AGV) navigation applications with strict real-time requirements, the most common solution consists in fusing together the information obtained by two different systems: (i) an on-board vehicle system, such as an odometer (i.e., an inertial navigation system), that offers estimation in the local robot frame (local localization); and (ii) an external positioning system, that provides position estimation in a absolute coordinates system (absolute localization). Nowadays, depending on the application domain, one can find several different solutions for the absolute localization problem. The simpler systems are based on the creation of artificial tracks, by means of

buried guide wires or optical beacons, that the AGV has to follows. More refined solutions allow the AGV to move relatively freely in the indoor environment. In this latter group of systems, one can find vision-based systems, laser navigation systems [13], and wireless positioning systems, such as frequency modulated continuous-wave or UWB. Today, laser-based systems are probably the most widely adopted, thanks to the high precision and reliability. Fusion of local and absolute position estimates can be carried out by Extended Kalman Filtering (EKF) [13] (or derived filters) or by sequential filtering techniques, such as particle filtering [12].

In this work, we present novel tracking systems based on the integration of a UWB-based absolute positioning system with a local positioning system constituted by the on-board odometer of a tricycle-like AGV. In order to take advantage of the intrinsic characteristics of UWB systems and to reduce the synchronization issues, we adopt a Time Differences of Arrivals (TDOA) approach for estimating the position of the AGV. In particular, we propose an innovative “Twin-receiver” TDOA (TTDOA) approach, in which two independent receivers are employed on the same AGV. In [2, 3], two distinct receivers are to directly estimate the AGV heading.

2 Extended Kalman Filter-Based Tracking

EKF is a classical tool of the estimation theory, often employed in the field of the real-time tracking of vehicles [8]. The EKF allows to predict and estimate the state $\mathbf{s} \in \mathbb{R}^n$, $n \in \mathbb{N}$ of a discrete-time controlled process governed by a non linear stochastic equation and affected by Gaussian noise. The EKF is composed by two steps: the *prediction step*, in which the future system state is predicted on the basis of the present state; and the *measurement step*, in which the prediction is refined by means of some indirect measurements of the system state, denoted as $\mathbf{z} \in \mathbb{R}^m$, $m \in \mathbb{N}$. In the following, the symbol $\overline{\bullet}$ is used to denote an *a priori* prediction of quantity \bullet , while the symbol $\hat{\bullet}$ is used to denote an *a posteriori* estimate of the quantity \bullet .

It is worth mentioning that, in both steps, the EKF uses an estimation of its error covariance matrix, denoted as \mathbf{P}_k , in order to refine its own prediction/estimation. In particular, in the measurement step it uses the *a priori* error covariance matrix $\overline{\mathbf{P}}_k = \mathbb{E}[(\mathbf{s}_k - \hat{\mathbf{s}}_k)(\mathbf{s}_k - \hat{\mathbf{s}}_k)^T]$, while in the prediction step it uses the *a posteriori* error covariance matrix $\hat{\mathbf{P}}_k = \mathbb{E}[(\mathbf{s}_k - \overline{\mathbf{s}}_k)(\mathbf{s}_k - \overline{\mathbf{s}}_k)^T]$.

2.1 The AGV and Its Mobility Model

The considered AGV, pictured in Fig. 1 (a), is a tricycle-like robot, with a two-wheel rear axis and a single wheel in the front axis, with both driving and steering functionalities. We make a distinction between the robot local frame (X_l and Y_l axes) and the absolute frame (X and Y axes). The heading of the vehicle θ coincides with the angle between the two reference systems, while α denotes the steering direction of the front wheel with respect to the X_l axis. We assume that the EKF estimates the position of the AGV taking the point of coordinates (x, y) as the Reference Point (RP). Since the distance between the front and the rear axes is given by L (dimension: [m]), the vehicle rotates the vehicle rotates around the Instantaneous Center of Rotation (ICR) with

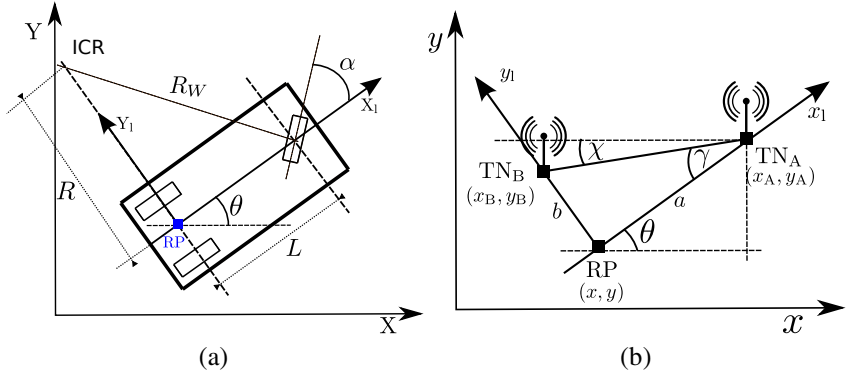


Fig. 1. (a) The pose of the considered AGV. (b) Position of the TN_A and TN_B with respect to the reference point.

a radius of curvature $R_w = L / \sin(\alpha)$, while it rotates around the origin of the robot local frame with a radius of curvature $R = L / \tan(\alpha)$. The state of the vehicle at the discrete time k is defined by the vector $\mathbf{s}_k \triangleq [x_k \ y_k \ \theta_k]^T$, with the following update equations [4]:

$$\begin{cases} x_{k+1} = x_k + T v_{sk} \cos(\theta_k) \cos(\alpha_k) \\ y_{k+1} = y_k + T v_{sk} \sin(\theta_k) \cos(\alpha_k) \\ \theta_{k+1} = \frac{T v_{sk}}{L} \sin(\alpha_k) \end{cases} \quad (1)$$

where T (dimension: [s]) is the sampling time, and $\{v_{sk}, \theta_k, \alpha_k\}$ are the measured speed, heading, and steering direction at epoch k .

2.2 Prediction Step

Before describing our specific system, we recall the general equations of the prediction step of the EKF [8]. Given the current system state estimation $\hat{\mathbf{s}}_{k-1}$, the prediction step to estimate the next state is

$$\bar{\mathbf{s}}_k = f(\hat{\mathbf{s}}_{k-1}, \mathbf{u}_k) + \mathbf{w}_{k-1} \quad (2)$$

where $f(\cdot, \cdot)$ is a generic non-linear function of the past system state and of the control input vector, denoted as \mathbf{u}^p , $p \in \mathbb{N}$. For the sake of simplicity, in (2) the dependence on the process noise $w \in \mathbb{R}^n$ is linear. Given that the noise covariance matrix is \mathbf{Q} , the a priori error covariance matrix can be derived as follows:

$$\bar{\mathbf{P}}_k = \mathbf{A} \hat{\mathbf{P}}_{k-1} \mathbf{A}^T + \mathbf{Q} \quad (3)$$

where $\mathbf{A} \triangleq \nabla_{\mathbf{s}} f|_{(\hat{\mathbf{s}}_{k-1}, \mathbf{u}_k, 0)}$.

In our case, the on-board odometer is the unique source of information. In particular, it provides, on average, every T^{odo} (dimension: [s]), two data to the on-board

controller:¹ (i) the linear displacement of the front wheel at the sampling time, denoted as S_k , and given by $T^o v_{sk}$ (dimension: [m]); (ii) the steering angle, denoted by α (dimension: [rad]). As shown in Section 2.1, the data coming from the odometer (i.e., the linear displacement of the front wheel and its steering angle) is sufficient to predict the future position and orientation of the vehicle in the absolute frame. Therefore, we use the odometer data as the system control input of equation (2), i.e., $\mathbf{u}_k = [S_k \alpha_k]^T$. Since the odometer measurements vector is affected by errors, we can define the vector $\tilde{\mathbf{u}}_k$ as follows:

$$\tilde{\mathbf{u}}_k = \begin{bmatrix} \tilde{S}_k \\ \tilde{\alpha}_k \end{bmatrix} = \begin{bmatrix} S_k + w'_k(1) \\ \alpha_k + w'_k(2) \end{bmatrix}. \quad (4)$$

where the vector $\mathbf{w}' = (w'_k(1), w'_k(2))$ is a bivariate Gaussian random vector with zero mean and with the following (known) covariance matrix:

$$\mathbf{Q}^{\text{odo}} = \begin{bmatrix} \sigma_S^2 & 0 \\ 0 & \sigma_\alpha^2 \end{bmatrix}.$$

By using equations (1) in equation (2), the following prediction equations of the EKF can be derived:

$$\begin{bmatrix} \bar{x}_k \\ \bar{y}_k \\ \bar{\theta}_k \end{bmatrix} = \begin{bmatrix} \hat{x}_{k-1} + \tilde{S}_k \cos(\hat{\theta}_{k-1}) \cos(\tilde{\alpha}_k) \\ \hat{y}_{k-1} + \tilde{S}_k \sin(\hat{\theta}_{k-1}) \cos(\tilde{\alpha}_k) \\ \hat{\theta}_{k-1} + \frac{\tilde{S}_k}{L} \sin(\tilde{\alpha}_k) \end{bmatrix} \quad (5)$$

In order to obtain the a priori error covariance matrix update equation (3), the matrix \mathbf{A} can be derived as previously shown, and the matrix \mathbf{Q} is related to the covariance matrix \mathbf{Q}^{odo} by the relationship $\mathbf{Q} = \mathbf{B} \mathbf{Q}^{\text{odo}} \mathbf{B}^T$, where

$$\mathbf{B} \triangleq \nabla_{\mathbf{u}} f|_{(\hat{s}_{k-1}, \mathbf{u}_k, \mathbf{0})} = \begin{bmatrix} \cos(\hat{\theta}_{k-1}) \cos(\alpha_k) - S_k \sin(\hat{\theta}_{k-1}) \sin(\alpha_k) \\ \sin(\hat{\theta}_{k-1}) \cos(\alpha_k) - S_k \cos(\hat{\theta}_{k-1}) \sin(\alpha_k) \\ \frac{\sin(\alpha_k)}{L} & \frac{S_k \cos(\alpha_k)}{L} \end{bmatrix}.$$

2.3 Measurement Step

The infrastructure UWB nodes of the positioning system, denoted as Anchor Nodes (ANs), have known positions. Additionally, ANs are assumed to be compliant with the IEEE 802.15.4a standard and to be synchronized by means of wired synchronization mechanisms.² The estimation of the AGV position is achieved by measuring the time of arrivals of suitable ranging IEEE 802.15.4a packets sent by the ANs nodes to the receivers installed on the AGV. As anticipated in Section 1, the AGV can have two different configurations: (a) the classical TDOA configuration with a single receiver; (b) the novel TTDOA configuration, that makes use of two independent receivers, each with its own antenna and its own independent clock generator. The receivers on board

¹ Even if practical odometers are typically affected by jitter, we ignore this issue in our work.

² Actually, the choice of the UWB technology is not restrictive, since in our system the only parameter related to the standard is the transmission time of the ranging packet.

of the AGV are denoted, respectively, as Target Node A (TN_A) and Target Node B (TN_B), and they are assumed to be *not synchronized* with each other and with the ANs.

The ANs transmit periodically—more precisely, every T^u (dimension: [s])—ranging packets that allow the TNs to estimate the distance between them. Clearly, the estimates are affected by noise (assumed to be Gaussian) and by a bias, due to the lack of synchronization with the ANs. As usual, this bias can be eliminated by computing the relative distances between the TNs and the ANs. The relative distances are obtained by subtracting the distance between the TNs and a Reference Node (RN), selected among the ANs, from the distance between the TNs and the AN. The ANs simultaneously transmitting to the AGV (i.e., in the same “collision domain”) are forced to transmit in orthogonal slot times in order to avoid interference. We assume that every collision domain contains 5 ANs and the EKF measurements’ update is performed as soon as all 5 ANs have sent their own ranging packets. We assume that Non-Line-of-Sight (NLOS) propagation conditions, which are highly detrimental for the system performance, are clearly identified by the AGV [7]. This strong assumption is quite realistic, as the AGV knows precisely its position and it also knows perfectly the surrounding industrial environment. Therefore, we assume that all the range estimates used by the EKF are obtained through Line-of-Sight (LOS) channels, without obstacles in any propagation path between the AN and the TNs. Observing that the bi-dimensional TDOA problem requires 4 pseudo-range measures to estimate the position without any ambiguity—as there are 5 ANs in each collision domain—the TDOA estimate is feasible also if one of the 5 ANs is in NLOS condition with respect to TN_A (and TN_B in the case of the TTDOA). We point out that when the number of LOS ANs, denoted as N , is smaller than 4, the measurement step is not performed and the system relies simply on the prediction step.

We now provide the measurement update equations. In particular, given that the measurement vector can be expressed as $\mathbf{z}_k = h(\mathbf{s}_k) + \mathbf{v}_k$, where $h(\cdot)$ is a non-linear function of the current system state and $\mathbf{v} \in \mathbb{R}^m$ is the measure noise with covariance matrix \mathbf{R} , the measurement update equations become

$$\hat{\mathbf{s}}_k = \bar{\mathbf{s}}_k + \mathbf{K}_k \mathbf{e}_k \quad \hat{\mathbf{P}}_k = (\mathbf{I}_n - \mathbf{K}_k \mathbf{H}) \bar{\mathbf{P}}_k$$

where the Kalman gain \mathbf{K}_k and the measurement error \mathbf{e}_k are defined as

$$\mathbf{e}_k = \tilde{\mathbf{z}} - \mathbf{H} \bar{\mathbf{s}}_k \quad \mathbf{K}_k = \frac{\bar{\mathbf{P}}_{k-1} \mathbf{H}^T}{\bar{\mathbf{P}}_{k-1} \mathbf{H}^T + \mathbf{R}}$$

where \mathbf{H} is the Jacobian of $h(\cdot)$ with respect to the state vector \mathbf{s} , i.e., $\mathbf{H} \triangleq \nabla_{\mathbf{h}|\mathbf{s}}|_{(\bar{\mathbf{s}}_k)}$, evaluated in $(\bar{\mathbf{s}}_k, \mathbf{0})$.

TDOA Method. The TDOA method is directly inspired by the approach presented in [11]. In particular, the non-linear TDOA problem is tackled by linearization, considering the distance between the TN and the RN to be known, using the state of the EKF itself. We remark that, in this case, we are actually using a KF, rather than an EKF. As shown in [4], the following update equations can be obtained:

$$\begin{aligned} \mathbf{e}_k &= \mathbf{z} - \mathbf{H}^{TDOA T} \bar{\mathbf{s}}_k = \mathbf{z} - \mathbf{u} - \hat{r}_1 \mathbf{p}_k & \mathbf{K}_k &= \frac{\bar{\mathbf{P}}_{k-1} \mathbf{H}^{TDOA T}}{\bar{\mathbf{P}}_{k-1} \mathbf{H}^{TDOA T} + \mathbf{R}^{TDOA}} \\ \hat{\mathbf{s}}_k &= \bar{\mathbf{s}}_k + \mathbf{K}_k \mathbf{e}_k & \hat{\mathbf{P}}_k &= (\mathbf{I}_{N-1} - \mathbf{K}_k \mathbf{H}^{TDOA}) \bar{\mathbf{P}}_k \end{aligned}$$

where \hat{r}_1 is the distance between the RN and the predicted AGV position $[\bar{s}_k(1), \bar{s}_k(2)]^T$. The expressions of the vectors and matrices (not shown here for lack of space) can be found in [4].

TTDOA Method. The TDOA method does not provide information about the heading θ of the vehicle. We now introduce the TTDOA technique, which, by employing two distinct UWB receivers, allows to reliably estimate the heading of the vehicle. The first receiver (TN_A) is located on the longitudinal axis of the AGV at coordinates $(a, 0)$. The second receiver (TN_B) is located on the traversal axis at the coordinates $(0, b)$ of the local frame. In Fig. 1 (b), it is possible to observe the positions of the receivers in the absolute frame, denoted, respectively, (x_A, y_A) and (x_B, y_B) , when the AGV is rotated by an angle θ . Therefore, the measurement equation provides an *indirect* estimation of θ and of the position of the RP, through direct estimation of the positions of the two TNs. The following update equations can be finally derived [4]:

$$\begin{aligned} \mathbf{e}_k &= \mathbf{z} - \mathbf{H}^{TTDOA}{}^T \bar{s}_k & \mathbf{K}_k &= \frac{\bar{\mathbf{P}}_{k-1} \mathbf{H}^{TTDOA}{}^T}{\bar{\mathbf{P}}_{k-1} \mathbf{H}^{TTDOA}{}^T + \mathbf{R}^{TTDOA}} \\ \hat{s}_k &= \bar{s}_k + \mathbf{K}_k \mathbf{e}_k & \hat{\mathbf{P}}_k &= (\mathbf{I}_4 - \mathbf{K}_k \mathbf{H}^{TTDOA}) \bar{\mathbf{P}}_k \end{aligned}$$

where the expressions of the vectors and matrices (not shown here for lack of space) can be found in [4].

3 Simulation Setup

3.1 Performance Metrics

The first considered performance metrics are the Root Mean Square Errors (RMSEs) of the estimated position and heading of the AGV:

$$RMSE_r = \sqrt{\mathbb{E}\{(\hat{x} - x)^2\} + \mathbb{E}\{(\hat{y} - y)^2\}} \quad RMSE_\theta = \sqrt{\mathbb{E}\{(\hat{\theta} - \theta)^2\}}.$$

Moreover, in order to assess the impact of the scenario geometry on the performance we consider the Geometric Dilution Of Precision (GDOP) and the Position Error Bound (PEB) [9]. Roughly speaking, the GDOP is an indicator of the impact of the geometry of the ANs on the position estimation errors, without considering the distance between ANs and TN. In the case of a TDOA system, it can be computed as in [10]:

$$GDOP_A^{TDOA} = \frac{1}{\sigma_{r_0}} \sqrt{\mathbf{G}_A(1, 1) + \mathbf{G}_A(2, 2)} \quad (6)$$

where \mathbf{G}_A indicates the matrix relative to the TN_A receiver and $\sigma_{r_0}^2$ is the ranging error (variance of the error in the estimated distance). It can be shown that the minimum GDOP, equal to $2/\sqrt{N}$, is obtained when the ANs build a regular polygon around the TN.

The GDOP becomes useless when the ranging error depends on the distance, since in this case the geometry of the network is less important. In this context, the PEB is more relevant, since it is defined as the lower bound of $RMSE_r$, thus allowing to

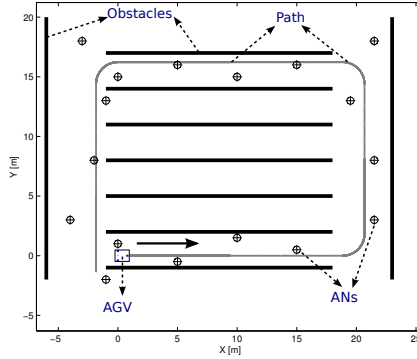


Fig. 2. The considered simulation scenario

assess the impact of both (i) the distances of the ANs from the TNs and (ii) the network geometry [9]. The expression of the PEB for a TOA system is [9]:

$$\text{PEB}_A^{\text{TOA}} = \sqrt{\frac{\sum_{k=1}^n A_k}{\sum_{k=1}^n A_k c_k \sum_{k=1}^n A_k s_k - (\sum_{k=1}^n A_k c_k s_k)^2}}$$

where

$$A_k = \frac{1}{\sigma_{r_0}^2 \|\text{TN}_A - \text{AN}_k\|^2} + \frac{2}{\|\text{TN}_A - \text{AN}_k\|^2} \quad (7)$$

$c_k = \cos(\theta_k^A)$, $s_k = \sin(\theta_k^A)$, θ_k^A is the angle between the x-axis of the absolute frame and the segment between the origin and TN_A , and $\|\text{TN}_A - \text{AN}_k\|$ is the length of the segment itself (the distance). We have considered the PEB for a TOA system since (i) it is easier to obtain than the PEB of a TDOA system and (ii) both PEBs are very similar, as shown in the simulation analysis carried out in Subsection 3.2. We finally observe that, in the case of constant σ_r , equation (7) reduces to $A_k = \sigma_{r_0}^{-2}$ and, then, the PEB becomes identical to the GDOP multiplied by σ_{r_0} , i.e., $\text{PEB}^{\text{TOA}} = \sigma_{r_0} \text{GDOP}^{\text{TOA}}$.

3.2 Description of the Scenario

The tracking algorithms presented in the previous sections have been evaluated using a custom Matlab-based simulator, considering the scenario shown in Fig. 2. The AGV (indicated by a rectangle) follows a predetermined path (solid gray line) in a warehouse-like environment. In particular, every T° (dimension: [s]), the AGV chooses its direction according to a simple path-following algorithm, and it generates a uniformly distributed speed in the interval $[v_s^{\min}, v_s^{\max}]$. For easy of comprehension, we preliminary remark that the AGV reaches (on average) the first turn at $t = 20$ s, the second turn at $t = 30$ s, and the third turn (North-West corner) at about $t = 50$ s. The considered bi-dimensional environment also has some obstacles (thick black lines), that absorb the UWB signal, thus leading to NLOS propagation conditions. The ANs (indicated by a cross and a circle) are pseudo-randomly placed. Before evaluating the performance of the TDOA

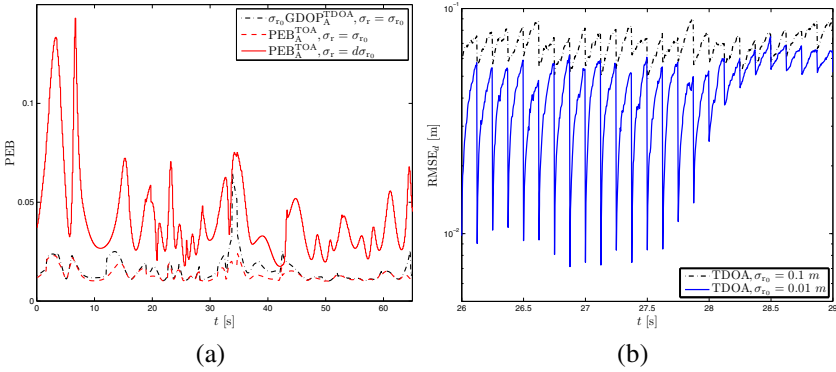


Fig. 3. (a) GDOP and PEB experienced by the AGV along the considered path. (b) RMSE_r as a function of time (and thus position), obtained with the TDOA algorithm. Two values of σ_{r_0} are considered (0.1 and 0.2 m).

Table 1. Parameters used in the simulation

Parameter	σ_s	σ_α	σ_{r_0}	T^o	T^u	L	a	b	v_s^{\max}	v_s^{\min}
Value	0.01 m	0.00175 rad	0.01 m	3.9 ms	125 ms	0.8 m	0.8 m	0.4 m	2.5 m/s	0.6 m/s

and TTDOA tracking algorithms, every receiver selects independently the nearest $N = 4$ ANs, always ignoring the more favorable case with $N = 5$ ANs. The nearest node is always designated as the RN.

In the simulation analysis, we have considered two cases. In the first, the ranging errors are independent from the distance between ANs and TNs, thus implying that $\sigma_{r_i} = \sigma_{r_0}$. This situation is slightly unrealistic, but it allows to emphasize the impact of the network geometry on the performance. Conversely, in the second case σ_{r_i} is directly proportional to the distance. In this case, the ranging error can be much larger than in the first case, thus yielding to larger position estimation errors. This intuition is confirmed by the PEB curves shown in Fig. 3 (a), obtained while the AGV follows the path of Fig. 2. We remark that the PEB^{TOA} curves are relative to a TOA system, but they compare favorably (by proper scaling) with the GDOP^{TDOA} curves of a TDOA system, shown in the same figure as a benchmark. Therefore, we can consider PEB^{TOA} as a good indicator of the real PEB^{TDOA}. When σ_{r_i} is constant, the PEB exhibits a unique relevant peak at $t = 35$ s, and this indicates that the ANs are well positioned. On the contrary, when σ_{r_i} is variable, the number of peaks and also their heights increase significantly. It is worth mentioning that the standard deviations σ_s and σ_α characterize the error generated by the odometer at every step, i.e., every T^o s. Therefore, in order to obtain the standard deviation of the error accumulated in a 1 m-path segment, it is necessary to divide σ_s and σ_α by $\sqrt{T^o v_s(t)}$. For example, using the values provided in Table 1, the standard deviation of the displacement accumulated in 1 m belong to the interval $[\sigma_s / \sqrt{T^o v_s^{\max}}, \sigma_s / \sqrt{T^o v_s^{\min}}] \simeq [0.1, 0.2]$ m. If not otherwise specified, the values of the relevant simulation parameters are those shown in Table 1. According to

these values, $T^o \ll T^u$ s, and this implies that the measurement step is executed with a significant lower frequency than the prediction step.

4 Simulation Results

In Fig. 3 (b), the RMSE_r of the EKF with the TDOA algorithm, measured at every prediction step (every T^o s), is shown as a function of time for a small portion (between 26 s and 29 s) of the trajectory of the AGV, in order to emphasize the interplay between the odometer and the UWB positioning system. In fact, the results shown in Fig. 3 (b) show clearly that the error accumulated by the odometer alone increases over time, till totally unreliable estimates are provided. However, using the UWB positioning system, even affected by an error of the same order of magnitude of that of the odometer, prevents the RMSE_r from drifting away. From Fig. 3 (b), it is also interesting to observe that undesirable oscillations of the estimation (and, thus, of the AGV position) occur only when the local and the absolute system have very different levels of accuracy.

In the upper and lower subfigures of Fig. 4 (a), RMSE_r and RMSE_θ, respectively, are shown as functions of time. In both cases, two values of $\sigma_{r_i} = \sigma_{r_0}$ are considered (namely, 0.1 m and 0.01 m). Fig. 4 (a) shows that the TTDOA approach, by taking advantage of the twin receiver configuration, significantly reduces both RMSE_r and RMSE_θ. More importantly, at least from the AGV point of view, the TTDOA approach also reduces the estimation oscillations, thus leading to a smoother AGV movement. Despite these improvements, the RMSEs still show a few peaks. They are due to the combination of several causes. Notably, the peak at $t = 25$ is probably due to the peak of the PEB observed in Fig. 3 (a). On the other hand, the remaining RMSE peaks appear in correspondence to the turns of the path and, therefore, are probably generated by the odometer. This is reasonable since, during turns, both the source of error (α and S) of the odometer have relevant impacts, while in the straight segment the error on α has

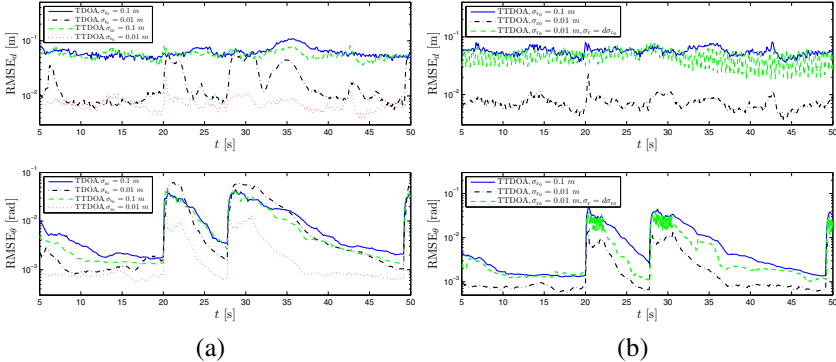


Fig. 4. (a) RMSE_r (upper subfigure) and RMSE_θ (lower subfigure), as functions of time, with the TDOA and the TTDOA algorithms, respectively. Two values of σ_{r_0} (0.1 m and 0.01 m) are considered. (b) RMSE_r (upper figure) and RMSE_θ (lower figure), as functions of time, using the TTDOA algorithm, considering the cases of fixed (0.1 m and 0.01 m) and variable ($\sigma_{r_0} = 0.01$ m) values of σ_{r_i} .

a limited impact. Moreover, when the speed of the AGV is smaller (as happens in the turns), there is a greater accumulated error.

We now consider a more realistic scenario, where σ_{r_i} is a function of the distance ($\sigma_{r_i} = d\sigma_{r_0}$), by considering only the TTDOA algorithm, as this is more promising than the traditional TDOA. In Fig. 4 (b), we compare the new scenario with the previous one, by setting $\sigma_{r_0} = 0.1$ m and $\sigma_{r_0} = 0.01$ m in the previous scenario and $\sigma_{r_0} = 0.01$ m in the new one. From the results in Fig. 4 (b), one can observe that: the performance of the TTDOA algorithm in the new scenario, in terms of RMSE_θ , is approximated by the performance in the previous scenario with $\sigma_{r_0} = 0.1$ m; instead, the performance in the new scenario, in terms of RMSE_θ , is close to the ideal one.

5 Conclusions

In this paper, we have presented two real-time tracking algorithms for an AGV moving in an industrial scenario, based on a EKF that combines measures from the on-board odometer and from a UWB-based absolute positioning system. In particular, the algorithm that uses a twin receiver configuration has shown to offer a cm-grade accuracy in realistic conditions. The main issue to deal with in next future consists in reducing the oscillations in the EKF position estimation, in order to smooth the movement of the AGV.

Acknowledgment

The work of S. Busanelli was supported by the Spinner consortium. The authors would like to thank F. De Mola, M. Magnani, and M. Casarini (all of Elettric80 Spa) for providing relevant information and for their continuous support and help.

References

1. Part 15.4: Wireless Medium Access Control (MAC) and Physical Layer (PHY) Specifications for Low-Rate Wireless Personal Area Networks (WPANs). Amendment 1: Add Alternate PHYs (August 2007)
2. Anderson, R., Bevly, D.: Estimation of slip angles using a model based estimator and GPS. In: Proceedings of the American Control Conference, Boston, MA, USA, vol. 3, pp. 2122–2127 (June 2004)
3. Bevly, D., Ryu, J., Gerdes, J.: Integrating INS sensors with GPS measurements for continuous estimation of vehicle sideslip, roll, and tire cornering stiffness. IEEE Transactions on Intelligent Transportation Systems 7(4), 483–493 (2006)
4. Busanelli, S., Ferrari, G.: UWB-based tracking of autonomous vehicles with multiple receivers: Extended analytical framework. Tech. rep., n. 2010-09-17-GF, Dept. of Inform. Eng., University of Parma, Italy. Available upon request (September 2010)
5. Gezici, S., Poor, H.: Position estimation via ultra-wideband signals. Proceedings of the IEEE 97(2), 386–403 (2009)
6. Gezici, S., Zhi, T., Giannakis, G.B., Kobayashi, H., Molisch, A.F., Poor, H.V., Sahinoglu, Z.: Localization via ultra-wideband radios: a look at positioning aspects for future sensor networks. IEEE Signal Processing Mag. 22(4), 70–84 (2005)

7. Guvenc, I., Chong, C.C., Watanabe, F., Inamura, H.: NLOS identification and weighted least-squares localization for UWB systems using multipath channel statistics. *EURASIP J. Adv. Signal Process* 2008, 36 (2008)
8. Haykin, S.: Adaptive filter theory. Prentice-Hall, Englewood Cliffs (2002)
9. Jourdan, D.B., Roy, N.: Optimal sensor placement for agent localization. *ACM Trans. Sen. Netw.* 4(3), 1–40 (2008)
10. Levanon, N.: Lowest GDOP in 2-D scenarios. *IEE Proceedings-Radar, Sonar and Navigation* 147(3), 149–155 (2000)
11. Nájar, M., Vidal, J.: Kalman tracking based on TDOA for UMTS mobile location. In: Proc. IEEE International Symposium on Personal and Indoor and Mobile Radio Commun., vol. 1, pp. B45–B49 (September 2001)
12. Rigatos, G.: Extended Kalman and particle filtering for sensor fusion in motion control of mobile robots. *Math. Comput. Simul.* (May 2010)
13. Teslić, L., Škrjanc, I., Klančar, G.: EKF-based localization of a wheeled mobile robot in structured environments. *Springer Journal of Intelligent and Robotic Systems*, 1–17 (June 2010)
14. Ubisense System Overview: <http://ubisense.net>
15. Win, M., Scholtz, R.: Impulse radio: how it works. *IEEE Commun. Letters* 2(2), 36–38 (1998)